Broadband Characterization of Dielectric Films for Power-Ground Decoupling

J. Obrzut and R. Nozaki[1]

NIST, Polymers Division
Gaithersburg, MD 20899-854, USA
Phone: +1 301 975-6845, Fax: +1 301 975-2938
Email: jan.obrzut@nist.gov

Abstract - **We evaluated the dielectric permittivity and impedance characteristics of high dielectric constant polymer composite films. Such materials are being investigated by the electronic industry in response to the growing need for efficient integrated power- ground de-coupling capacitance in microwave circuits and fast switching devices. In order to extend the dielectric measurements to the microwave range, we developed an appropriate expression for the input admittance of a thin film capacitance terminating a coaxial line. The theoretical model treats the capacitance as a distributed network and takes into consideration the wave propagation in the specimen section. The dielectric permittivity of several high dielectric constant materials for de-coupling capacitance applications was evaluated at frequencies of 100 MHz to 10 GHz, and the corresponding impedance characteristics were determined directly in time domain. Polymer resins filled with ferroelectric ceramics showed low impedance values and flat impedance characteristics over a broad frequency range, which makes these materials attractive for power-ground decoupling applications in high-speed electronic circuits.**

Keywords - **dielectric permittivity, decoupling capacitance, broadband measurements, coaxial discontinuity, microwave characterization, TDR.**

I. INTRODUCTION

The need for power - ground de-coupling is nearly universal in electronic circuits to secure signal integrity and reduce electromagnetic interference noise. Current technologies utilize surface mounted discrete chip capacitors, which can effectively extinguish the power-bus noise at frequencies below 10 MHz. At higher frequencies, between 10 MHz and 100 MHz, only capacitors with the lowest connection inductance are able to source the charge. As the operating frequency increases above several hundred MHz, all the discrete capacitors become ineffective and the voltage driving device level can be stabilized solely by the inter-plane capacitance [1]. Composites of polymer resins filled with high-dielectric constant ceramics may be useful in constructing embedded de-coupling capacitance (EDC) and power planes with desirable, low impedance characteristics over a broad frequency range, including the microwave [2]. Advancing EDC technology requires a suitable test method to measure the materials dielectric properties and to assess the impedance characteristic in planar, thin film configuration

over a broad frequency range. The existing broadband test procedures for film specimens assume no propagation in the specimen section [3]. They fail to produce meaningful results at frequencies above few hundred megahertz [4], especially in the case of high-dielectric constant films. A mode matching analysis was proposed for two-layer structures with the assumption that only higher order TM modes propagate in the specimen section [5]. This model, however, is not readily extendable to thin non-conducting films where TE rather than TM modes dominate the wave propagation.

In this paper we describe a measurement methodology that takes into consideration the wave propagation in the specimen section. Using the new test technique, the dielectric permittivity of several industry-developed high-dielectric constant films was accurately evaluated at frequencies of 100 MHz to 10 GHz, and the impedance characteristics were determined directly using the time domain reflectometry. Based on these results, the desirable dielectric characteristics are discussed from the viewpoint of designing efficient embedded de-coupling capacitance.

II. THEORETICAL ANALYSIS

The experimental arrangement under consideration is shown in Figure 1. A dielectric circular film (disk) specimen of thickness t is placed at the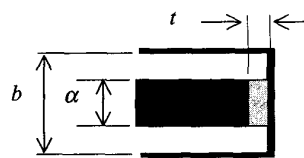 end of the center conductor of a coaxial airline. The diameter of the specimen a matches that of the center conductor. The specimen is covered with the counter conductor directly extending from the outer conductor and forms a circular

Fig. 1 Diagram of the test fixture

parallel-plate capacitor terminating the coaxial line. The incoming transverse-electromagnetic (TEM) wave approaches the sample section through the coaxial line. It has been commonly assumed that the lumped capacitance model applies to this structure at higher frequencies and still satisfies the quasi-static conditions as long as the length of the propagating wave is much larger than the film

[1]Permanent address: Division of Physics, Graduate School of Science, Hokkaido University, Sapporo 0810, Japan.

thickness [6]. Such an assumption implies that the propagation direction in the specimen section continues to be parallel to the coaxial line, across the specimen thickness. Since the specimen is short terminated, the wave should be reflected back after a delay time of $\tau \approx 2t\sqrt{\varepsilon'}/c$. For a circular film specimen having the diameter of 3.0 mm with a thickness of 100 µm and ε' of about 39, this double passing delay time would have been within 4 ps. In fact, the time delay measured for such specimen in a TDR experiment is in the range of about 62 ps consistent with $\tau \approx a\sqrt{\varepsilon'}/c$. The delay time depends on the diameter of the specimen rather than on its thickness. Thus, when the film thickness is much smaller than its diameter, $t \ll a$, the primary propagation mode satisfying the boundary conditions in the specimen section is associated with a single passing along the diameter of the film specimen. The structure in Fig.1 is therefore electrically equivalent to a network in which the dielectric film can be viewed as a transmission line inserted between two matched transmission lines. Consequently, the scattering coefficient S_{11}, resulting from the combination of the wave multiple reflection and transmission components in the specimen section, can be expressed by the following equation [7]:

$$S_{11} = \rho + \sum_{n=1}^{\infty} (-\rho e^{-\gamma a})^{n-1} (1-\rho^2) e^{-\gamma a} = \frac{\rho + e^{-\gamma a}}{1 - \rho e^{-\gamma a}} \quad (1)$$

where, ρ is the complex reflection coefficient for non-magnetic media; $\rho = (1 - \sqrt{\varepsilon^*})/(1 + \sqrt{\varepsilon^*})$, γ is the propagation constant; $\gamma = \frac{j\omega}{c}\sqrt{\varepsilon^*}$, ε^* is the relative complex permittivity of the dielectric, $\varepsilon^* = \varepsilon' - j\varepsilon''$, ω is an angular frequency and c is the speed of light in air.

The input admittance of the specimen section Y_{in}, having characteristic conductance of G_s, can be expressed in terms of the circuit parameters where the specimen represents an unmatched termination whose reflection coefficient is Γ.

$$Y_{in} = G_s \frac{1-\Gamma}{1+\Gamma} \quad (2)$$

Since a matched load follows the termination, the scattering coefficient, S_{11}, equals Γ.

Combining equation (1) with (2) leads to equation (3):

$$Y_{in} = G_s \frac{(1-\rho)(1-e^{-\gamma a})}{(1+\rho)(1+e^{-\gamma a})} \quad (3)$$

Introducing $x = \frac{\omega a}{2c}\sqrt{\varepsilon^*}$ equation (3) can be expressed as:

$$Y_{in} = G_s \frac{j\omega a}{2c}\varepsilon^* \frac{1}{x\cot(x)} \quad (4)$$

The specimen section in equation (4) is represented as a transmission line having an electrical length of $a/2$. In the complex capacitance notation, the characteristic conductance per unit of length represents the geometric capacitance C_p of the specimen, $C^* = G_s \frac{a}{2c}\varepsilon^* = C_p \varepsilon^*$. The term $1/x\cot(x)$ accounts for the wave propagation in the specimen section. If the electrical length is small in comparison to the wavelength, $a \ll \lambda$, $x \ll 1$, the value of the $x\cot(x)$ approaches unity and (4) simplifies to the conventional expression for the input admittance of a transmission line terminated with a lumped shunt capacitance [3].

During measurements, the reference plane is set at the interface between the end of the coaxial line having the characteristic conductance G_l and the dielectric specimen section with the characteristic conductance G_s. According to [6, 8] a cell constant parameter, G_s/G_l, can be determined by evaluating the fringing field capacitance C_f around the specimen section:

$$C^* = C_p\varepsilon^* + C_f = \frac{\pi a^2}{4t}\varepsilon_0\varepsilon^* + 2a\varepsilon_0 \ln\left(\frac{b-a}{2t}\right) \quad (5)$$

Using the fringing field capacitance (5) and equation (4), we finally arrive at equation (6) for the complex permittivity of the film specimen:

$$\varepsilon^* = \frac{G_l}{j\omega C_p} \frac{1 - S_{11}^m}{1 + S_{11}^m} \cdot x\cot(x) - \frac{C_f}{C_p} \quad (6)$$

where S_{11}^m is the measured scattering coefficient, C_p is the geometric capacitance of the empty specimen section, C_f represents the fringing field capacitance, a and b are the diameters of the center and outer conductor, respectively, as shown in Fig. 1, t is the specimen thickness, ε_0 is the permittivity of air and x is the propagation parameter defined the same as in equation (4). The value of the C_f/C_p ratio depends on the configuration of the specimen section and decreases to zero with decreasing film thickness.

Equation (6) is an entangled expression containing complex permittivity ε^* on both sides. Therefore, an iterative algorithm is required to find the value of ε^*, satisfying equation (6) for each measured value of S_{11}^m. It can be noted that at sufficiently low frequencies, the term $x\cot(x)$ approaches unity with $x \approx 0$, and equation (5) simplifies to (7), the conventional lumped element model [3],

$$\varepsilon^* = \frac{G_l}{j\omega C_p} \cdot \frac{1-S_{11}^m}{1+S_{11}^m} - \frac{C_f}{C_p} \quad (7)$$

which can be used for initial guessing of the complex permittivity values at low frequencies.

III.   EXPERIMENTAL

The broadband measurements were conducted using an experimental coaxial test fixture constructed from two APC–7 mm to APC–3.5 mm microwave adapters. The center conductor was replaced with a fixed 3.0 mm diameter pin, machined precisely to achieve flat and parallel contact between the film specimen and the APC–7 mm short termination. In comparison to other fixtures that utilize coaxial connectors or coupling probes, this compact test fixture minimizes radiation losses, coupling errors and errors caused by inductive components.

High dielectric constant EDC films: EDC-1, EDC-2, EDC-3 (Epoxy resins ferroelectric ceramics composites) and EDC-4 (Polyimide ferroelectric ceramic composite) were obtained from the NCMS Embedded Capacitance Project [2]. The dielectric properties determined for these materials using a microstrip resonator technique are listed in Table I. The circular film specimens with a 3.0 mm diameter were defined

Table I
Dielectric properties, ε' and tan (δ), of the EDC films of thickness t, measured at resonant frequency f.

Material	t (μm)	f (GHz)	ε'	tan (δ)
EDC-1	50	0.928	3.88	0.02
EDC-2	100	0.842	38.6	0.03
EDC-3	8	1.012	22.1	0.08
EDC-4	48	1.093	11.8	0.01

by photolithography.

Dielectric measurements in frequency domain were carried out in the frequency range between 100 MHz and 10 GHz using a network analyzer (HP 8720D). One-port S_{11} (open, short and broadband load) calibration was performed using a HP 85050B APC-7 calibration kit. The relative combined

standard uncertainty in geometrical capacitance measurements was typically 2 % with the primary contribution from the uncertainty in the film thickness measurements. The relative standard uncertainty of S_{11} was assumed to be within the manufacturer's specification for the HP 8720D. The combined relative experimental uncertainty in complex permittivity was less than 8 % while the experimental resolution of the dielectric loss tangent measurements was about 0.01. The time domain reflectometry (TDR) measurements were carried out using a Tektronix 11802 Digital Sampling Oscilloscope equipped with a TEK SD-24 TDR/Sampling Head. Waveforms were captured in a 10 ns window typically containing 1024 data points with a resolution of 2.5 ps. The relative combined standard uncertainty of the impedance determined in time domain was about 5 %.

IV   RESULTS AND DISCUSSION

Example measurements of the frequency dependent dielectric constant, ε', and the dielectric loss ε'' obtained for the EDC films are plotted in Fig. 2 and 3. The results obtained from the lumped element model without propagation (equation 7) are also plotted for comparison.
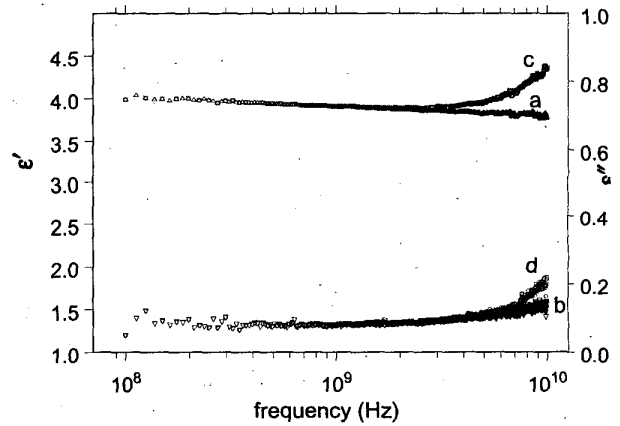

Fig. 2. Dielectric permittivity of EDC-1; a) dielectric constant, b) dielectric loss, c) and d) dielectric constant and dielectric loss obtained using the lumped capacitance method.

The permittivity results obtained for the EDC-1 and EDC-2 films agree well with the microstrip resonance data (Tab. 1) where the differences are within 1 % for ε' and 4 % for ε''. Equation (6) correctly calculates complex permittivity of the EDC films throughout the entire frequency range of 100 MHz to 10 GHz. The dielectric constant of EDC-1 is about 4.0 at 100 MHz and decreases to about 3.8 at 5 GHz, which is a typical dispersion behavior observed for epoxy resins. The dielectric loss data shown in Fig. 2b are in the range of about 0.08 to 0.1 and are also consistent with the dielectric

properties of FR–4 epoxy based laminates. The dielectric permittivity of the EDC-2 films shown in Fig. 3 is approximately 10 times larger than that of EDC-1, which results from the ferroelectric ceramics.

The ε' of EDC-2 decreases from about 40 at 100 MHz to about 39 at 5 GHz while the dielectric loss (Fig. 3b) increases from about 0.4 to 1.8 with increasing frequency, which agrees
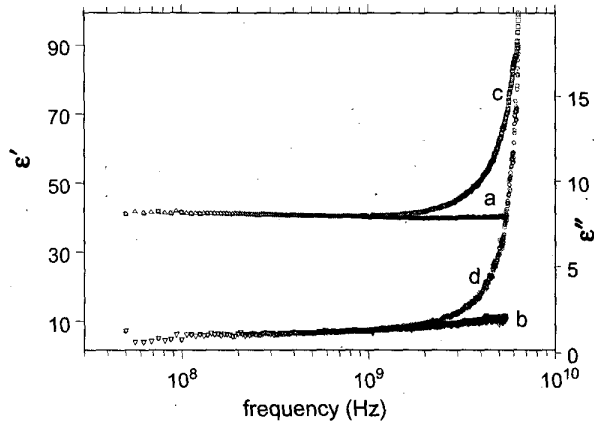

Fig. 3. Dielectric permittivity of EDC-2; a) dielectric constant,
b) dielectric loss, c) and d) dielectric constant and dielectric loss obtained according to the lumped capacitance method.

well with the microstrip resonance data. Results shown in Fig. 2 and 3 indicate that the new model, in which the film specimen is treated as a distributed component with capacitance, correctly describes the complex permittivity of low and high dielectric constant films over a broad frequency range. In contrast, the lumped element model shows anomalies at frequencies above 1 GHz to 3GHz (see Fig. 2c, 2d and 3c, 3d). The value of the real part of permittivity, ε', and the imaginary part, ε", determined from the lumped element model, increase as frequency increases, leading to systematic errors that at higher frequencies considerably exceed the combined experimental uncertainty. The relative systematic uncertainty of the lumped element method, Δ_{ls}^{*}, may be expressed as a ratio of equations (7) and (6):

$$\Delta_{ls}^{*} = \frac{1}{x\cot(x)} - 1 \qquad (8)$$

It can be noted that expression (6) has a singularity when $x = \pi/2$, which corresponds to a half-wavelength resonance at frequency f_r:

$$f_r = \frac{c}{2a\sqrt{\varepsilon^{*}}} \qquad (8)$$

The resonant frequency depends on the diameter of the film specimen and its complex permittivity. The systematic errors become larger as the dielectric constant of the film specimen increases. For film samples with finite dielectric loss, the real part of Δ_{ls}^{*} undergoes an oscillation reaching zero at the resonant frequency, while the imaginary part shows a peak value at that frequency.

Fig. 4 shows the impedance characteristics determined from the TDR response reflected at the EDC film specimens terminating the coaxial test fixture (Fig. 1). The measurements are normalized to the 50 Ω impedance of a precision coaxial airline. It is seen that at the delay time τ_o (or at highest frequencies ω) all the EDC specimens appear as a short circuit indicating a pure capacitive behavior. At longer times, the voltage builds up across the complex capacitance $C_p \varepsilon^{*}$ increasing its impedance until it effectively becomes an open circuit. An inductive delay, which is a common source of error in impedance measurements, does not visibly contribute to the measured response. The implemented coaxial test fixture configuration together with the propagation model allow accurate impedance measurements that satisfy the requirements in characterization of thin film dielectrics and low impedance substrates for the de-coupling functions.

The best performance is indicated by the response close to that of zero impedance (short) termination, as it is shown in Fig. 4b for EDC-3. In comparison to the other EDC materials
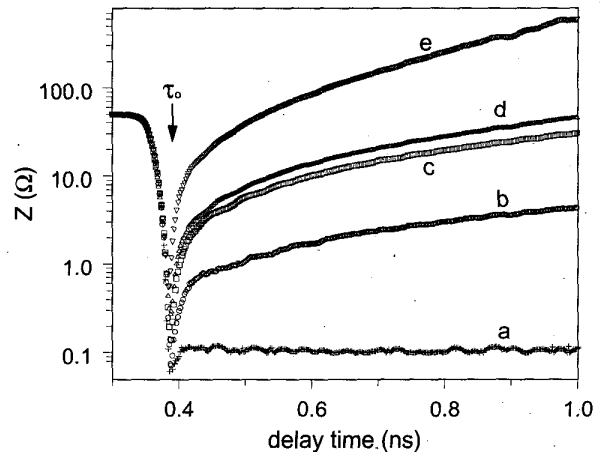

Fig. 4. Impedance of the EDC films measured in time domain: a) short termination, b) EDC-3 c) EDC-2, d) EDC-4 and e) EDC-1.

tested, the 8 μm thick EDC-3 film had the highest geometric capacitance C_p, which compensated its somewhat lower dielectric constant than that of EDC-2 (Tab. 1). For the same geometric capacitance, lower impedance will result from a dielectric material with higher complex permittivity ε^{*}.

In order to provide an adequate amount of charge and eliminate transient depressions in the voltage driving device level, the EDC impedance should be low ($Z_{EDC} \approx 0$) at a broad range of frequencies. In Fig 4, the 3.0 mm diameter test capacitor can source the charge as long as its impedance is lower than the reference input impedance. This requirement can be realized by decreasing the dielectric thickness between the planes and increasing the dielectric permittivity of the inter-plane dielectric. At frequencies approaching 1 GHz and above, the EDC plane in a circuit board is no longer electrically small and typically exhibits undesired rapid oscillation of impedance at resonant frequencies. Since the magnitude of oscillation depends on the quality factor Q, the resonant behavior can be suppressed by introducing a loss mechanism into the EDC material as a frequency tailored dielectric loss and/or conductor loss. Both the dielectric loss and the conductor loss contribute to lowering the broadband impedance.

The EDC materials measured in a functional test vehicle configuration showed very flat impedance characteristics, indicating a much lower Q factor than could be expected from the dielectric properties of the organic and ceramic constituents. Our study indicates that organic polymer resins filled with ferroelectric powder exhibit an intrinsic high frequency loss. We found that the position of the loss peak is determined by the dielectric relaxation of the polymer backbone while its magnitude depends on the materials dielectric dispersion and, therefore, is amplified by the content and permittivity of the ferroelectric component. A polymer matrix with shorter relaxation time shifts the loss peak position to higher frequencies, while higher polarizability can increase the loss magnitude. In most organic polymers, molecular relaxations cease at frequencies above a few gigahertz. To suppress the resonant behavior at frequencies beyond the molecular relaxation, a conductor loss may be introduced in the form of a semi-conducting layer at the metal dielectric interface. For example, a layer of copper oxide, which is a typical surface modifier to promote adhesion between a copper conductor and a polymer resin in copper-cladded epoxy laminates, can be used to attenuate higher-order resonant modes.

V.   CONCLUSION

Dielectric permittivity and impedance characteristics of embedded de-coupling capacitance films were evaluated in time domain and at frequencies ranging from 100 MHz to 10 GHz. At those frequencies, the film specimen terminating coaxial line was treated as a network consisting of a transmission line with a capacitance, for which we developed a suitable propagation model. The new testing methodology eliminates systematic errors associated with the existing lumped element models and enables broadband measurements of permittivity at frequencies of practical importance, namely above 1 GHz. The accuracy of the dielectric loss is not compromised by the thin film configuration, since the propagation direction was found to be along the diameter of the specimen rather that across the film thickness. In addition, the coaxial test fixture configuration minimizes the coupling errors, errors caused by inductive components and radiation losses. The presented testing technique is attractive not only for standardized measurements, but also for scientific research. It was found that polymer composite films filled with ferroelectric ceramics could provide low impedance through a high capacitance and an intrinsic high frequency relaxation process.

The corresponding high frequency loss can effectively suppress a resonant behavior and eliminate electromagnetic noise in the power bus. This makes polymer composite films very attractive for embedded de-coupling capacitance and low impedance power planes in high-speed electronic circuits.

REFERENCES

1. T. Hubbing and M.Xu, "Electronic design considerations for printed circuit boards with embedded capacitance", Proceedings of the NCMS Conference on Embedded Capacitance, February 28-29, 2000, Tempe AZ, USA
2. P. Lee and R. Chabornneau (Ed.), Embedded Capacitance Project Report, NCMS, 3025 Boardwalk, Ann Arbor, MI 48108, August, 2000.
3. M. A. Stuchly and S. S. Stuchly, "Coaxial line reflection methods for measuring dielectric properties of biological substances at radio and microwave frequencies: A review", IEEE Trans. on Instrum. Meas., vol. 29, pp 176-83, 1980.
4. F. I. Mopsik, "Extended frequency range dielectric measurements of thin films", Rev. Sci. Instrum. vol.71, pp. 2456-2460, 2000.
5. N. Beldhadj-Tahar, O. Mayer and A. Fourrier-Lamer, "Broad-band microwave characterization of bi-layerd materials using a coaxial discontinuity with applications for thin conductive films for microelectronics and material in air-tight cell", IEEE Trans. on Microwave Theory Tech., vol. 45, pp. 260-67, 1997.
6. N. Marcuvitz, Waveguide Handbook. McGraw-Hill, New York: 1951.
7. R. Nozaki and J. Obrzut, "Broadband complex permittivity measurements of solid films at microwave frequencies", microwave frequencies", unpublished.
8. M. F. Iskander and S. S. Stuchly, "Fringing field effect in the lumped-capacitance method for permittivity measurements", IEEE Trans. on Instrum. Meas., vol. 27, pp. 107-109, 1978.